Corrected 20 February 2018. See full text.

ORGANOIDS

Patient-derived organoids model treatment response of metastatic gastrointestinal cancers

**Georgios Vlachogiannis,[1] Somaieh Hedayat,[1] Alexandra Vatsiou,[2] Yann Jamin,[3] Javier Fernández-Mateos,[1,2] Khurum Khan,[1,4] Andrea Lampis,[1] Katherine Eason,[1] Ian Huntingford,[1] Rosemary Burke,[5] Mihaela Rata,[3] Dow-Mu Koh,[3,6] Nina Tunariu,[3,6] David Collins,[3] Sanna Hulkki-Wilson,[1] Chanthirika Ragulan,[1] Inmaculada Spiteri,[2] Sing Yu Moorcraft,[4] Ian Chau,[4] Sheela Rao,[4] David Watkins,[4] Nicos Fotiadis,[6] Maria Bali,[3,6] Mahnaz Darvish-Damavandi,[1] Hazel Lote,[1,4] Zakaria Eltahir,[1] Elizabeth C. Smyth,[4] Ruwaida Begum,[4] Paul A. Clarke,[5] Jens C. Hahne,[1] Mitchell Dowsett,[7] Johann de Bono,[8] Paul Workman,[5] Anguraj Sadanandam,[1] Matteo Fassan,[9] Owen J. Sansom,[10] Suzanne Eccles,[5] Naureen Starling,[4] Chiara Braconi,[4,5] Andrea Sottoriva,[2] Simon P. Robinson,[3] David Cunningham,[4] Nicola Valeri[1,4]*

Patient-derived organoids (PDOs) have recently emerged as robust preclinical models; however, their potential to predict clinical outcomes in patients has remained unclear. We report on a living biobank of PDOs from metastatic, heavily pretreated colorectal and gastroesophageal cancer patients recruited in phase 1/2 clinical trials. Phenotypic and genotypic profiling of PDOs showed a high degree of similarity to the original patient tumors. Molecular profiling of tumor organoids was matched to drug-screening results, suggesting that PDOs could complement existing approaches in defining cancer vulnerabilities and improving treatment responses. We compared responses to anticancer agents ex vivo in organoids and PDO-based orthotopic mouse tumor xenograft models with the responses of the patients in clinical trials. Our data suggest that PDOs can recapitulate patient responses in the clinic and could be implemented in personalized medicine programs.

High-throughput sequencing has been extensively used in precision medicine to identify somatic mutations that can be exploited for cancer treatment and drug development (*1*). However, the limited role of genomic profiling in predicting response to targeted therapies and the limitations of preclinical models used for drug validation are important obstacles hampering the success of personalized medicine (*2*). Co-clinical trials are parallel studies in which drug responses in patients are matched to laboratory preclinical models to personalize treatment and understand mechanisms of chemosensitivity through functional genomics and reverse translation (*3*). Most co-clinical trials rely on the use of genetically engineered mouse models or patient-derived xenografts, posing logistic, ethical, and economic issues (*4*).

LGR5$^+$ stem cells can be isolated from a number of organs and propagated as epithelial organoids in vitro to study physiology and neoplastic transformation (*5*). Most studies on human colorectal cancer (CRC) organoids have been conducted on cultures derived from primary tumors (*6*). In contrast, examples of PDOs from metastatic cancer sites remain sparse (*7*–*9*). Furthermore, very limited evidence is available on the ability of PDOs to predict response to treatment in the clinic (*10*). Here we present a living biobank of PDOs from heavily pretreated metastatic gastrointestinal cancer patients and show examples of how the drug responses of these cancer organoids can be compared with those of the actual patient.

A total of 110 fresh biopsies from 71 patients enrolled in four prospective phase 1/2 clinical trials were processed between October 2014 and February 2017. In line with previous data (*7*), PDOs were grown from 70% of biopsies with a cellularity of 2+ and above, and their establishment rate strongly correlated with tumor cellularity in the parental biopsy (χ^2 test, $P < 0.0001$). No inverse correlation was observed between PDO establishment rate and presence of necrosis (cutoff ≥ 20%). Tumor percentage is a key limiting factor for genomic and transcriptomic analyses. When the 60% threshold used in large sequencing studies of primary CRC (*11*) or gastroesophageal cancer (GOC) (*12*) was applied in our cohort, we found no correlation between PDO take-up rate and tumor percentage, suggesting that PDOs can also be established in cases of a low tumor/stroma ratio, thus allowing the ex vivo expansion of the cancer population in samples that would have otherwise failed quality-control tests for next-generation sequencing (NGS).

PDOs presented in this study were derived from ultrasound ($n = 20$), computed tomography (CT)–guided ($n = 7$), or endoscopic ($n = 2$) biopsies of metastatic CRC (mCRC; $n = 16$), metastatic GOC (mGOC; $n = 4$), and metastatic cholangiocarcinoma ($n = 1$) patients (fig. S1). Liver, pelvic, peritoneal, and nodal metastases of chemorefractory patients were used to establish PDOs. In several cases, PDOs were established from sequential biopsies at baseline (BL), at the time of best response [partial response (PR) or stable disease (SD)], and at the time of disease progression (PD), as well as from multiregion biopsies (table S1).

Histological evaluation revealed notable morphological similarities between PDOs and the patient biopsies from which they were originally derived (Fig. 1, A and B, and figs. S2A and S2B). Immunohistochemistry markers routinely used in the diagnosis of CRC (CDX-2 and CK7) showed that the parental tumor's expression pattern was maintained in PDOs, even when derived from sequential biopsies during treatment (fig. S2, C to E). Similarly, amplification of oncogenic drivers such as *ERBB2* (Fig. 1C and fig. S2F) and rearrangements in *FGFR2* (fig. S2G) were retained in PDOs from mGOC and metastatic cholangiocarcinoma, respectively.

NGS was used to profile 151 cancer-related genes in both PDOs ($n = 23$) and their parental biopsies; archival material from primary cancer or pretreatment diagnostic biopsies was also sequenced for eight patients, and whole-genome sequencing (WGS) was performed for one PDO (tables S2 and S3). The molecular landscape of our PDOs (Fig. 1D) largely overlapped with that reported for mCRC and mGOC in the MSK-IMPACT study (*1*), with the exception of *SRC* and *EGFR* amplifications and *ATM* and *BRCA2* mutations that were more frequent in our mCRC PDO cohort (table S4). Overall, a 96% overlap in mutational spectrum was observed between PDOs and their parental biopsies (Fig. 1D), whereas intratumor heterogeneity was observed between archival material (primary cancer) and metastatic deposits (biopsies or PDOs) (fig. S3A and table S2). PDOs were able to capture spatiotemporal intratumor heterogeneity when established from multiple biopsies at the time of disease progression and when compared with PDOs established at the beginning of treatment (Fig. 1D, fig. S3A, and table S2). Similar results were observed for copy number alterations (CNAs) in PDOs and biopsies collected at different time points during treatment (figs. S3B and S4). WGS confirmed CNAs extrapolated from targeted NGS of PDOs or PDO-derived orthotopic tumors (PDO-xenografts) (figs. S3B and S4); CNAs detected in key oncogenic

[1]Division of Molecular Pathology, The Institute of Cancer Research, London, UK. [2]Centre for Evolution and Cancer, The Institute of Cancer Research, London, UK. [3]Cancer Research UK Cancer Imaging Centre, Division of Radiotherapy and Imaging, The Institute of Cancer Research and Royal Marsden Hospital, London, UK. [4]Department of Medicine, The Royal Marsden NHS Trust, London, UK. [5]Cancer Research UK Cancer Therapeutics Unit, The Institute of Cancer Research, London, UK. [6]Department of Radiology, The Royal Marsden NHS Trust, London, UK. [7]Ralph Lauren Centre for Breast Cancer Research, Royal Marsden Hospital NHS Trust, London, UK. [8]Division of Clinical Studies, The Institute of Cancer Research, London, UK. [9]Department of Medicine, Surgical Pathology and Cytopathology Unit, University of Padua, Padua, Italy. [10]Cancer Research UK Beatson Institute, Glasgow, UK.
*Corresponding author. Email: nicola.valeri@icr.ac.uk

Corrected 20 February 2018. See full text.

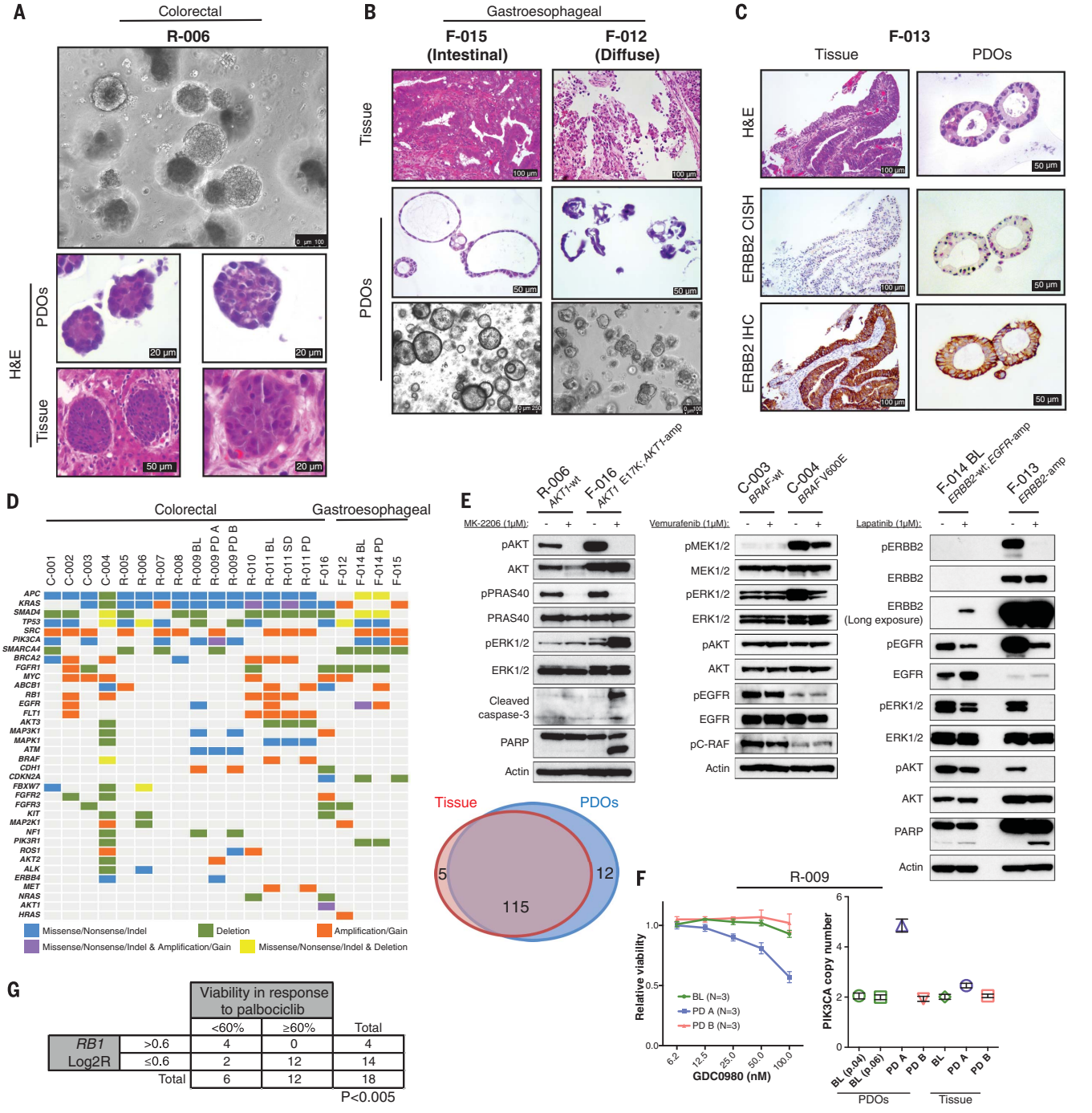

G

		Viability in response to palbociclib		
		<60%	≥60%	Total
RB1 Log2R	>0.6	4	0	4
	≤0.6	2	12	14
	Total	6	12	18

P<0.005

Fig. 1. Histopathological, molecular, and functional characterization of patient-derived organoids (PDOs). (**A**) Phase-contrast image of a mCRC PDO culture (top) and hematoxylin and eosin staining comparing organoids to their matching patient biopsy (bottom). (**B**) Intestinal and diffuse growth patterns are retained in mGOC PDOs. (**C**) *ERBB2* amplification and overexpression in mGOC PDOs and parental tissue biopsy (CISH, chromogenic in situ hybridization; IHC, immunohistochemistry). (**D**) Heatmap showing the most frequently mutated and/or copy number–altered genes in PDOs (left) and Venn diagram demonstrating 96% mutational overlap between PDOs and parental tissue biopsies (right). (**E**) Target engagement in genotype–drug phenotype combinations: pathway analysis downstream of ERBB2 in *ERBB2*-amplified and nonamplified PDOs treated with lapatinib (24 hours) (right), BRAF inhibition (24 hours) (center), and AKT inhibition (4 hours) (left). wt, wild type. (**F**) Concentration-dependent effect of the dual PI3K/mTOR inhibitor GDC-0980 in three PDOs from patient R-009, all carrying an acquired PIK3CA mutation (H1047R). PDOs established from a liver metastasis biopsied at disease progression (R-009 PD-A) that also harbored *PIK3CA* amplification showed concentration-dependent response to GDC-0980. *PIK3CA*-mutant but nonamplified PDOs established before regorafenib treatment (R-009 BL) or from a different liver metastasis biopsied at disease progression (R-009 PD-B) did not respond to GDC-0980. Viability data shown are means ± SEM of indicated independent experiments. (**G**) Correlation (Fisher's exact test) between presence of *RB1* amplification in PDOs (D) and response to the CDK4/CDK6 inhibitor palbociclib in the reported drug screen (fig. S9A). BL, baseline; SD, stable disease; PD, posttreatment/progressive disease.

Corrected 20 February 2018. See full text.

drivers were further validated by digital-droplet polymerase chain reaction (fig. S5). High concordance was observed in mutational, CNA, and transcriptomic profiling over successive passages when PDOs were tested before and after several months of continuous culture [passage range, 5 to 13; mutations, coefficient of determination (R^2) = 0.96, $P < 0.0001$; CNA, $R^2 = 0.97$, $P < 0.0001$; gene expression (RNA sequencing), $R^2 = 0.7$, $P < 0.001$] (fig. S6).

Next we tested the feasibility of using PDOs derived from metastatic cancers as drug-screening tools and validated the robustness of our approach by identifying several genotype–drug phenotype correlations across the PDO panel. We ran three-dimensional (3D) screening assays over a period of 2 weeks (figs. S7 and S8), using a library of 55 drugs now in phase 1 to 3 clinical trials or in clinical practice (table S5). The heatmap shown in fig. S9A summarizes the screening data; hit validation at lower drug concentrations is reported in fig. S9B. For all 19 screens, a very high correlation was observed among each screen's three replicate assays and controls (fig. S10).

F-013 was the only *ERBB2*-amplified PDO in our cohort (Fig. 1C), and it exhibited the strongest response to lapatinib [dual ERBB2/epidermal growth factor receptor (EGFR) inhibitor]; lapatinib potently inhibited the mitogen-activated protein kinase (MAPK) and phosphatidylinositol 3-kinase (PI3K)/AKT signaling downstream of EGFR/ERBB2, inducing apoptosis in the F-013 PDO (Fig. 1E and fig. S9A). In a PDO (F-014) in which *EGFR* was amplified but *ERBB2* was not, lapatinib had no effect on viability and only modestly reduced MAPK and PI3K/AKT signaling (Fig. 1E and fig. S9A).

Similarly, across all PDOs, F-016 was the only tumor carrying an *AKT1* amplification and E17K mutation (E, glutamic acid; K, lysine) (Fig. 1D) and was the only one to respond strongly to both AKT inhibitors present in the drug library (MK-2206

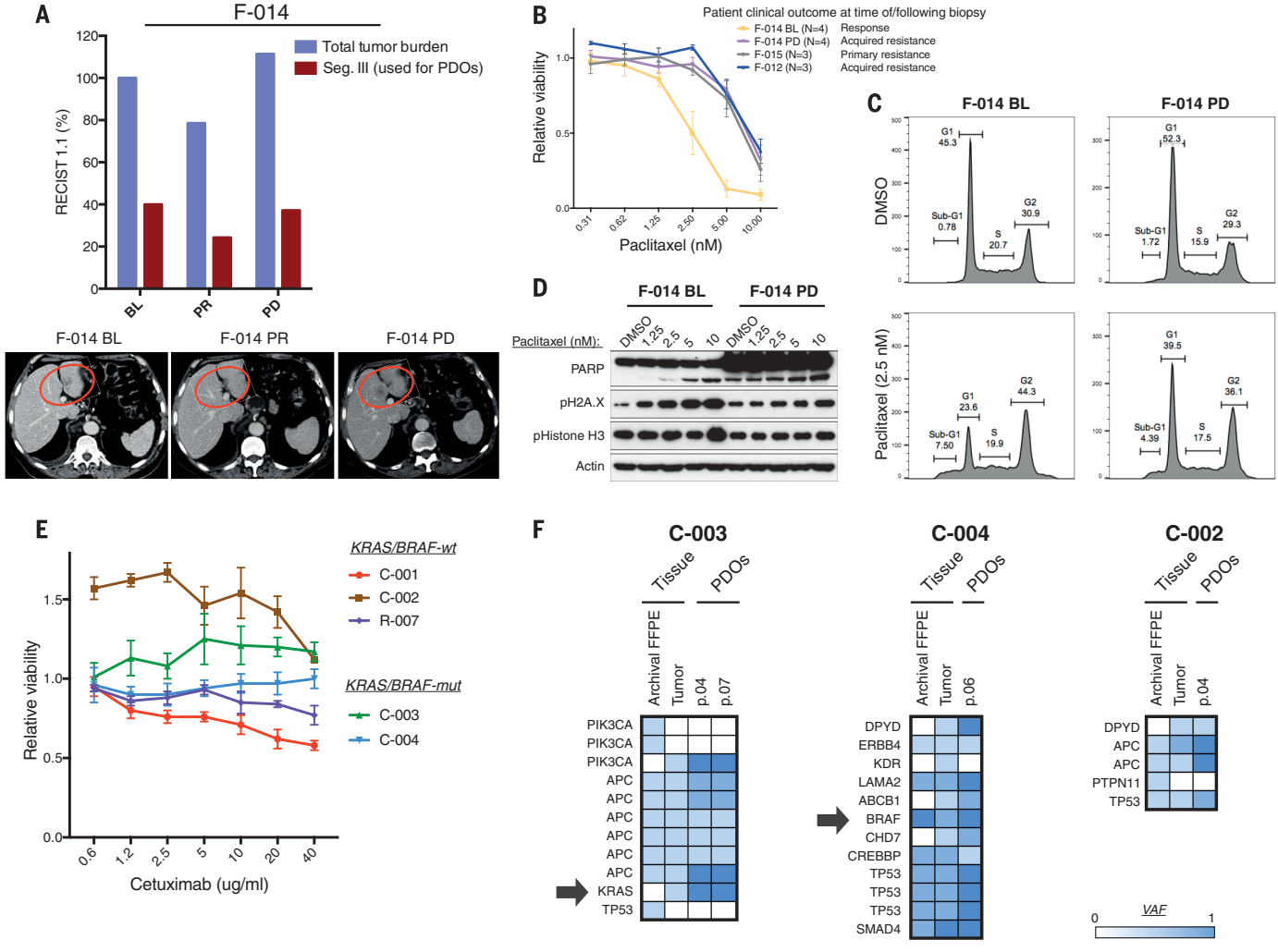

Fig. 2. PDO-based ex vivo co-clinical trials in mGOC and mCRC. (**A**) PDOs were generated from sequential biopsies of a liver metastasis (red circles in the bottom panel) of mGOC patient F-014 that showed initial response to paclitaxel (F-014 BL) and subsequently progressed (F-014 PD). Violet bars indicate overall tumor volume [according to RECIST (Response Evaluation Criteria in Solid Tumors) 1.1], and red bars indicate volume of the target metastasis used to generate PDOs. (**B**) Cell viability upon paclitaxel treatment was compared in BL and PD PDOs from patient F-014 and PDOs from patients that exhibited primary (F-015) or acquired (F-012) resistance to paclitaxel in the clinic. Viability data shown are means ± SEM of indicated independent experiments. (**C**) Cell cycle analysis upon paclitaxel treatment in the F-014 BL PDO compared with the F-014 PD PDO. DMSO, dimethyl sulfoxide. (**D**) Concentration-dependent DNA damage was observed in the F-014 BL PDO in response to paclitaxel but not in PDOs from the same patient established at PD. (**E**) PDOs were established from BL (C-003 and C-004) and PD (C-001 and C-002) biopsies from patients treated with the anti-EGFR monoclonal antibody cetuximab. PDOs were treated with cetuximab in vitro; data shown are means ± SD from independent experiments performed in triplicate. (**F**) Molecular analysis of BL and PD PDOs, matching biopsy (tumor), and primary bowel cancer (archival); arrows indicate the presence of clonal or subclonal mutations in *BRAF* or *KRAS*, respectively, in two patients. VAF, variant allele frequency; FFPE, formalin-fixed paraffin-embedded.

Corrected 20 February 2018. See full text.

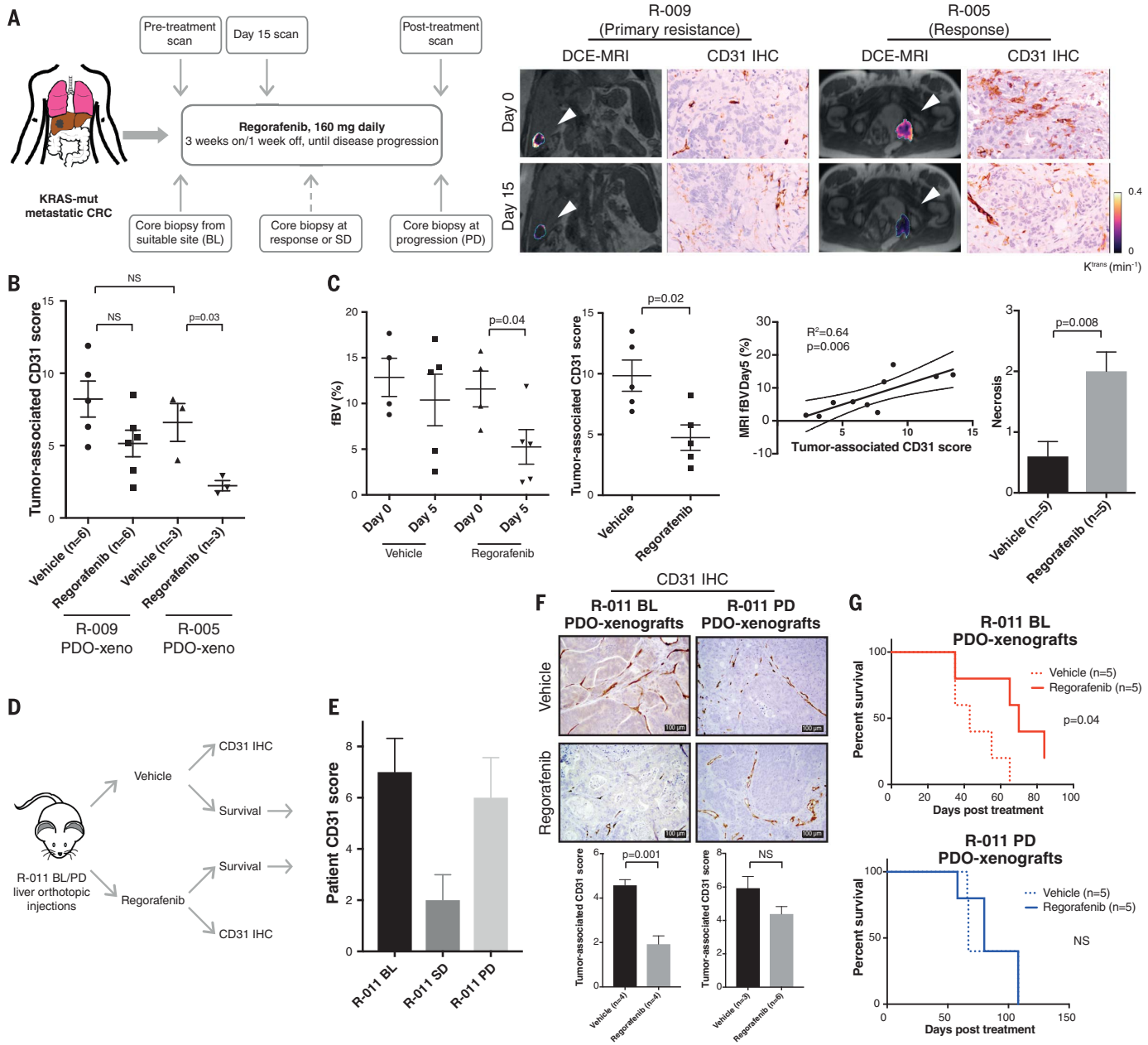

Fig. 3. PDO-based co-clinical trials mimic primary and acquired resistance to regorafenib in mice. (**A**) mCRC patients on regorafenib treatment underwent biopsies at BL, SD, or PD. An early reduction (15 days) in functional imaging (DCE-MRI) parameters correlated with changes in microvasculature assessed by CD31 staining and clinical benefit from regorafenib (right). Arrowheads indicate CRC metastases; K^{trans}, volume transfer constant. (**B**) Changes in microvasculature in response to regorafenib were assessed in PDO-xenografts in mice by quantification of tumor-associated CD31-positive vessels. Data show PDO-xenografts from a primary resistant patient (R-009) and a long-term responder (R-005) to regorafenib. Means ± SD from the indicated number of mice (*n*) in a representative experiment are shown; significance was determined using Student's unpaired *t* test. (**C**) Reduction in fractional blood volume (fBV) in regorafenib-treated mice carrying long-term regorafenib responder (R-005) PDO-xenografts. A total of 10 animals were analyzed (five in each arm); shown are the means ± SD of an individual experiment. Day 0 fBV values could not be obtained for two animals owing to respiratory movement. Significance was determined using Student's paired *t* test for fBV and unpaired *t* test for CD31 and necrosis. (**D**) Schematic representation of the animal experiment using PDOs from patient R-011, established pre- and posttreatment with regorafenib. Mice carrying liver orthotopic R-011 pretreatment (BL) and posttreatment (PD) PDO-xenografts were randomized to control and treatment arms and treated with vehicle or regorafenib for 10 days. After treatment, each arm was further randomized to a cohort culled for histopathological analysis and a survival cohort, which was monitored over time. (**E**) CD31 immunostaining in the parental patient BL, SD, and PD biopsies, demonstrating an initial reduction in tumor microvasculature in response to regorafenib. Shown are means ± SD calculated by scoring 10 high-power-field tumor areas. (**F**) Representative images (top) and analysis (bottom) of CD31 immunostaining in the BL and PD R-011 PDO-xenografts. Shown are means ± SD calculated by scoring at least 10 high-power-field tumor areas per animal in an individual experiment; *n*, number of animals analyzed in each group. Significance was determined using Student's unpaired *t* test. (**G**) Kaplan-Mayer curves for regorafenib- or vehicle-treated mice bearing BL and PD PDO-xenografts from patient R-011 from an individual experiment (*n*, number of mice analyzed). Significance was determined using the Mantel-Cox log-rank test.

Corrected 20 February 2018. See full text.

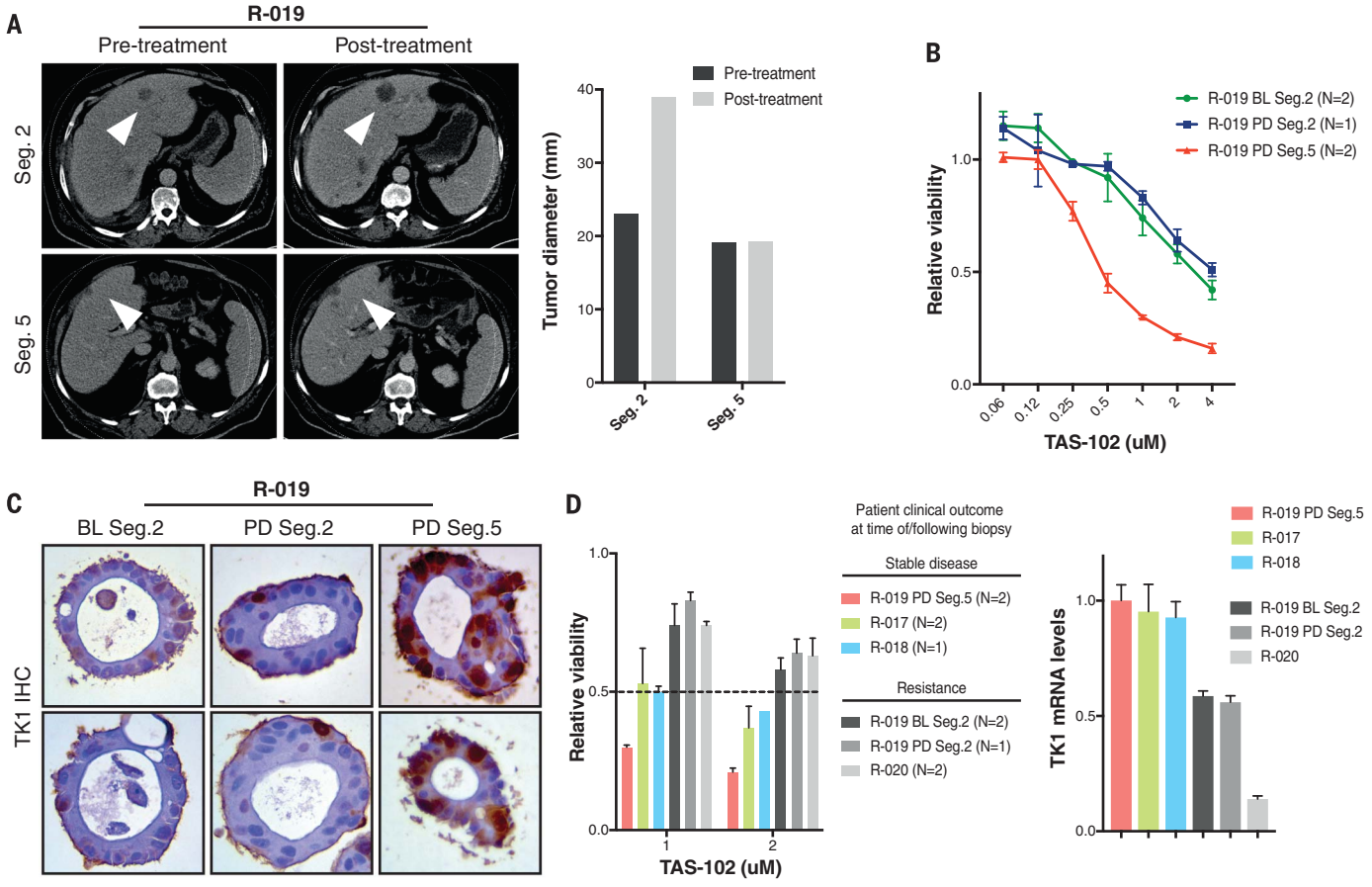

Fig. 4. PDOs recapitulate intra- and interpatient heterogeneity in response to TAS-102. (**A**) PDOs were established from a patient (R-019) with mixed response to TAS-102. Whereas the segment 2 metastasis rapidly progressed, the segment 5 metastasis remained stable upon TAS-102 treatment (white arrowheads in the CT scan indicate metastases; bars represent pre- and posttreatment measurements of the indicated metastases). (**B**) Ex vivo concentration-response curves in BL and PD multiregion PDOs from patient R-019 (with mixed response to TAS-102). (**C**) TK1 IHC expression in TAS-102–refractory (segment 2) and –sensitive (segment 5) PDOs. (**D**) Cell viability (left) and TK1 mRNA expression (right) in PDOs from TAS-102–responsive and –refractory patients. In (B) and (D), *N* indicates the number of independent experiments, and viability values are expressed as means ± SEM.

and GSK690693) (Fig. 1E and fig. S9A). One mCRC PDO (C-004) harbored a BRAF V600E mutation (V, valine) (Fig. 1D) and was the only PDO that showed significantly decreased viability after treatment with the BRAF inhibitor vemurafenib (fig. S9A). Consistent with this, vemurafenib selectively inhibited MEK/ERK (MAPK kinase/extracellular signal–regulated kinase) signaling in the C-004 PDO (Fig. 1E) but failed to induce apoptosis, in keeping with the lack of efficacy of single-agent BRAF inhibitors in mCRC (*13*).

Overall, *PIK3CA* mutations were not predictive of response to GDC-0980 (a dual PI3K/mTOR inhibitor) in the PDOs panel (Fig. 1D and fig. S9A). In line with this observation, in a patient from whom pre- and posttreatment PDOs were established from multiple metastases (R-009 BL, PD-A, and PD-B), a PIK3CA H1047R mutation (H, histidine; R, arginine) common to all the PDOs was not associated with any response to GDC-0980. However, PDOs carrying a synchronous *PIK3CA* amplification (R-009 PD-A) showed a concentration-dependent reduction in cell viability in response to GDC-0980 (Fig. 1F and fig. S3A). Last, in keeping with published data (*14*), a significant correlation was observed between *RB1* amplification and sensitivity of PDOs to palbociclib [cyclin-dependent kinase 4 (CDK4)/CDK6 inhibitor] (Fig. 1G).

After extensive molecular and functional characterization of our PDOs, we examined their clinical predictive value in 21 comparisons of clinical responses observed in patients with ex vivo response data gathered in organoids (table S6). Taxanes are a standard second-line treatment option for metastatic gastric cancer; however, efficacy is modest, and no predictive biomarkers are available to inform clinical decisions (*15*). We compared response to paclitaxel in sequential PDOs established before and after treatment in a paclitaxel-sensitive patient (F-014) with that in PDOs established from liver metastases of two paclitaxel-resistant patients (Fig. 2, A and B). PDOs derived from the responsive metastasis showed a GI_{50} (concentration that inhibits growth of cancer cells by 50%) for clinically relevant paclitaxel concentrations (*16*) that was about one-fourth that for PDOs from the same patient derived at progression; these resistant PDOs demonstrated an identical paclitaxel concentration-response profile to the two PDOs established from paclitaxel-refractory patients (Fig. 2B). Cell cycle analysis showed marked apoptosis and G_2 arrest upon taxane treatment in the pretreatment F-014 PDOs, whereas no significant difference was observed in PDOs established at progression (Fig. 2C and fig. S11A). Similarly, paclitaxel induced concentration-dependent DNA damage, mitotic arrest, and apoptosis in the pretreatment F-014 PDOs but had a much weaker impact on the progression (and thus resistant) PDOs (Fig. 2D). Consistent with data observed for second-line treatment, a ~10-fold difference in GI_{50} was observed in response to the combination of 5-fluorouracil and cisplatin in PDOs collected from chemosensitive and chemorefractory mGOC patients receiving first-line treatment (fig. S11B), highlighting the clinical potential of PDOs for treatment selection in cancers of unmet need.

Anti-EGFR monoclonal antibodies, regorafenib, and TAS-102 are U.S. Food and Drug Administration–approved options for treatment of chemorefractory mCRC; however, with the exception of RAS pathway

Corrected 20 February 2018. See full text.

mutations for anti-EGFR therapy, there are no validated clinical biomarkers for patient selection in this setting. We initially tested the predictive value of PDOs in mCRC by comparing response to anti-EGFR treatment (cetuximab) in five PDOs and their respective patients (Fig. 2E). Two PDOs established from BL biopsies before anti-EGFR treatment in the PROSPECT-C trial showed no response to cetuximab, in keeping with the primary resistance observed in these two patients in the clinic. Unsurprisingly (*17*), both PDOs and their respective patient biopsies harbored either *KRAS* G12D (subclonal) (G, glycine; D, aspartic acid) or *BRAF* V600E (clonal) mutations (Fig. 2F). The third cetuximab-resistant PDO (C-002) was established from the progression biopsy of a patient who initially responded to cetuximab, and it harbored an *EGFR* amplification (Fig. 1D and fig. S5), no RAS pathway mutational aberrations (Fig. 2F), and high amphiregulin mRNA levels. Despite these molecular markers being suggestive of responsiveness to cetuximab, the C-002 PDO showed no response (and, in fact, paradoxically showed enhanced proliferation) upon cetuximab treatment, in line with the respective patient's clinical outcome, thus highlighting the potential of PDOs to predict clinical outcomes better than molecular pathology alone. Another *KRAS* wild-type PDO derived from a slow-growing progressing metastasis in a patient with otherwise stable disease (C-001) (fig. S11C) showed a marginal response to cetuximab. Last, the *KRAS* wild-type PDO established from a BL biopsy of a patient enrolled in the PROSPECT-R trial (R-007) (fig. S11C) showed response to cetuximab at concentrations higher than 5 μg/ml; this, however, could not be compared with clinical response, because the patient did not receive anti-EGFR monoclonal antibodies.

Next we tested the ability of PDOs to recapitulate response to regorafenib, a multiple tyrosine kinase inhibitor blocking oncogenic and angiogenic signaling pathways. No response to regorafenib was observed in our 3D ex vivo screening assays (fig. S9A), an observation in keeping with our recently reported clinical results from the PROSPECT-R trial (*18*), suggesting that response to regorafenib is mainly driven by its anti-angiogenic effect (Fig. 3A).

To match responses to regorafenib in the clinic and in aligned PDOs, we established an orthotopic human tumor xenograft model by implanting luciferase-expressing (Luc^+) PDOs in the liver of NSG mice (PDO-xenografts) (fig. S12A). We initially compared response to regorafenib in PDO-xenografts from a patient with primary resistance (R-009; $n = 11$) and from a patient who achieved a durable (10-month) response (R-005; $n = 6$) to regorafenib (fig. S12, B and C). In keeping with the clinical responses (Fig. 3A), PDO-xenografts from the regorafenib-sensitive patient displayed a significant ($P = 0.03$) reduction in their microvasculature in response to regorafenib, as revealed by CD31 immunostaining; in contrast, no significant changes were observed in PDO-xenografts from the regorafenib-resistant patient (Fig. 3B). To mimic our clinical observations, we performed functional susceptibility contrast magnetic resonance imaging (MRI) of PDO-xenografts of the responding patient (R-005; $n = 10$) before and after treatment (fig. S12D). In line with dynamic contrast-enhanced MRI (DCE-MRI) results in patients (Fig. 3A), susceptibility contrast MRI revealed a significant reduction in tumor fractional blood volume (fBV) in regorafenib-treated mice (Fig. 3C). These changes were associated with a reduction in CD31 staining and increased necrosis (Fig. 3C). Notably, across all animals, a robust correlation was observed between the fBV values obtained from susceptibility contrast MRI and the microvasculature assessment (CD31) of the same samples ($R^2 = 0.64$, $P = 0.006$) (Fig. 3C). Consistent with our clinical data, changes in microvasculature indicative of response appeared to be independent of changes in tumor volume (fig. S12E) (*18*). Three different histopathological growth patterns (HGPs)—desmoplastic HGP, pushing HGP, and replacement HGP—have been associated with different degrees of response to anti-angiogenic drugs, with the replacement HGP being frequently associated with vessel co-option and primary resistance (*19*). In our experiments, a predominance of replacement HGP, and thus vessel co-option, was observed in PDO-xenografts from the resistant patient, whereas tumors established from the PDOs of the sensitive patient showed a prevalence of desmoplastic and pushing HGPs (fig. S12F), suggesting that vessel co-option might be the mechanism underpinning primary resistance to regorafenib. When the responder to regorafenib (R-005) progressed and received subsequent treatment, he was enrolled in a phase 1 trial of the ATR inhibitor VX-970. No response was observed in this patient with VX-970 monotherapy, and this was in keeping with the lack of response to ATM/ATR inhibitors observed in his PDOs in the drug screening reported in fig. S9A.

To test the PDOs' ability to capture tumor evolution and acquired resistance to treatment, we generated xenografts using PDOs from the same liver metastasis before (BL) and after (PD) treatment in mCRC patient R-011 that exhibited initial response to regorafenib and subsequently progressed (fig. S13A). Mice were randomized to treatment and control arms, and, after treatment, each arm was further randomized for survival or functional analysis (Fig. 3D). In line with clinical findings (Fig. 3E) (*18*), CD31 immunostaining revealed a ~60% reduction in microvasculature in response to regorafenib in BL PDO-xenografts ($P = 0.001$), whereas no significant change was observed in PD PDO-xenografts (Fig. 3F). More importantly, regorafenib treatment offered a selective survival benefit in mice carrying BL PDO-xenografts (Fig. 3G and fig. S13B), confirming the predictive value of PDOs and their ability to reflect cancer evolution upon treatment.

TAS-102, a combination of the nucleoside analog trifluridine and the thymidine phosphorylase inhibitor tipiracil, is approved for the treatment of chemorefractory mCRC, but no validated biomarkers are available (*20*). We compared clinical and preclinical response to TAS-102 in six organoids from four different patients treated with TAS-102. Initially, we tested response to TAS-102 in PDOs from a patient (R-019) who had a mixed response, with stability of disease in one of the liver metastases (segment 5) and rapid progression in another (segment 2) (Fig. 4A). Ex vivo concentration-response data showed about an eightfold difference in GI_{50} between PDOs derived from the TAS-102–sensitive metastasis and those derived from pre- and posttreatment biopsy of the rapidly progressing metastasis (Fig. 4B), highlighting the ability of PDOs to recapitulate intrapatient heterogeneity. TK1 has been proposed as a potential biomarker of response to TAS-102 (*21*); TK1 protein expression was indeed higher in PDOs from the responding metastasis than in those from the nonresponding site (Fig. 4C). When we extended the TAS-102 sensitivity analysis to PDOs from three other patients, we confirmed that PDOs from patients who achieved disease control were sensitive to low micromolar concentrations of TAS-102, whereas no significant effect on cell viability was observed in PDOs from resistant (primary or acquired) patients (Fig. 4D, left); consistent with previous data, TK1 mRNA expression was higher in PDOs from patients that achieved stable disease in response to TAS-102 (Fig. 4D, right).

Overall, for the PDOs that we analyzed, we found 100% sensitivity, 93% specificity, 88% positive predictive value, and 100% negative predictive value in forecasting response to targeted agents or chemotherapy in patients (Fisher's exact test, $P < 0.0001$) (table S7). Our data suggest that PDOs can be exploited for functional genomics to simulate cancer behavior ex vivo and integrate molecular pathology into the decision-making process of early-phase clinical trials.

REFERENCES AND NOTES

1. A. Zehir *et al.*, *Nat. Med.* **23**, 703–713 (2017).
2. E. E. Voest, R. Bernards, *Cancer Discov.* **6**, 130–132 (2016).
3. A. T. Byrne *et al.*, *Nat. Rev. Cancer* **17**, 254–268 (2017).
4. J. G. Clohessy, P. P. Pandolfi, *Nat. Rev. Clin. Oncol.* **12**, 491–498 (2015).
5. A. L. Bredenoord, H. Clevers, J. A. Knoblich, *Science* **355**, eaaf9414 (2017).
6. M. van de Wetering *et al.*, *Cell* **161**, 933–945 (2015).
7. F. Weeber *et al.*, *Proc. Natl. Acad. Sci. U.S.A.* **112**, 13308–13311 (2015).
8. M. Fujii *et al.*, *Cell Stem Cell* **18**, 827–838 (2016).
9. C. Pauli *et al.*, *Cancer Discov.* **7**, 462–477 (2017).
10. J. F. Dekkers *et al.*, *Sci. Transl. Med.* **8**, 344ra84 (2016).
11. Cancer Genome Atlas Network, *Nature* **487**, 330–337 (2012).
12. Cancer Genome Atlas Research Network, *Nature* **513**, 202–209 (2014).
13. D. M. Hyman *et al.*, *N. Engl. J. Med.* **373**, 726–736 (2015).
14. C. J. Sherr, D. Beach, G. I. Shapiro, *Cancer Discov.* **6**, 353–367 (2016).
15. E. C. Smyth *et al.*, *Ann. Oncol.* **27**, v38–v49 (2016).
16. L. M. Zasadil *et al.*, *Sci. Transl. Med.* **6**, 229ra43 (2014).
17. C. S. Verissimo *et al.*, *eLife* **5**, e18489 (2016).
18. K. Khan *et al.*, *Gut* 10.1136/gutjnl-2017-314178 (2017).
19. S. Frentzas *et al.*, *Nat. Med.* **22**, 1294–1302 (2016).
20. R. J. Mayer *et al.*, *N. Engl. J. Med.* **372**, 1909–1919 (2015).
21. Y. Kuboki *et al.*, *Lancet Oncol.* **18**, 1172–1181 (2017).

ACKNOWLEDGMENTS

This work was supported by Cancer Research UK (grant number CEA A18052), the National Institute for Health Research (NIHR) Biomedical Research Centre (BRC) at The Royal Marsden NHS Foundation Trust and The Institute of Cancer Research

Corrected 20 February 2018. See full text.

(grant numbers A62, A100, A101, and A159), and the European Union Seventh Framework Programme (grant number CIG 334261) to N.V.; by Cancer Research UK (C52506/A22909) to A.So.; by a Wellcome Trust grant (105104/Z/14/Z) to the Centre for Evolution and Cancer; by Cancer Research UK Cancer Imaging Centre funding (C1060/A16464) to The Institute of Cancer Research; by Cancer Research UK Programme Grants C309/A11566 and C2739/A22897 to the Cancer Therapeutics Unit of The Institute of Cancer Research; and by a Bayer Oncology Group Research Grant to D.Cu. A.So. is supported by The Chris Rokos Fellowship in Evolution and Cancer. I.C. has had advisory roles with Merck Serono, Roche, Sanofi Oncology, Bristol Myers Squibb, Eli Lilly, Novartis, and Gilead Science; has received research funding from Merck-Serono, Novartis, Roche, and Sanofi Oncology; and has received honoraria from Roche, Sanofi-Oncology, Eli Lilly, and Taiho. D.Cu. has received research funding from Roche, Amgen, Celgene, Sanofi, Merck Serono, Novartis, AstraZeneca, Bayer, Merrimack, and MedImmune. All other authors declare no conflicts of interest. The data presented in this paper are tabulated in the main text and supplementary materials. Sharing of materials is subject to a material transfer agreement with The Institute of Cancer Research, London (please direct requests to N.V.).

SUPPLEMENTARY MATERIALS

www.sciencemag.org/content/359/6378/920/suppl/DC1
Materials and Methods
Supplementary Text
Figs. S1 to S13
Tables S1 to S8
References (*22*–*34*)

4 July 2017; resubmitted 26 October 2017
Accepted 11 January 2018
10.1126/science.aao2774

Patient-derived organoids model treatment response of metastatic gastrointestinal cancers

Georgios Vlachogiannis, Somaieh Hedayat, Alexandra Vatsiou, Yann Jamin, Javier Fernández-Mateos, Khurum Khan, Andrea Lampis, Katherine Eason, Ian Huntingford, Rosemary Burke, Mihaela Rata, Dow-Mu Koh, Nina Tunariu, David Collins, Sanna Hulkki-Wilson, Chanthirika Ragulan, Inmaculada Spiteri, Sing Yu Moorcraft, Ian Chau, Sheela Rao, David Watkins, Nicos Fotiadis, Maria Bali, Mahnaz Darvish-Damavandi, Hazel Lote, Zakaria Eltahir, Elizabeth C. Smyth, Ruwaida Begum, Paul A. Clarke, Jens C. Hahne, Mitchell Dowsett, Johann de Bono, Paul Workman, Anguraj Sadanandam, Matteo Fassan, Owen J. Sansom, Suzanne Eccles, Naureen Starling, Chiara Braconi, Andrea Sottoriva, Simon P. Robinson, David Cunningham, and Nicola Valeri

Science **359** (6378), . DOI: 10.1126/science.aao2774

Cancer organoids to model therapy response

Cancer organoids are miniature, three-dimensional cell culture models that can be made from primary patient tumors and studied in the laboratory. Vlachogiannis *et al.* asked whether such "tumor-in-a-dish" approaches can be used to predict drug responses in the clinic. They generated a live organoid biobank from patients with metastatic gastrointestinal cancer who had previously been enrolled in phase I or II clinical trials. This allowed the authors to compare organoid drug responses with how the patient actually responded in the clinic. Encouragingly, the organoids had similar molecular profiles to those of the patient tumor, reinforcing their value as a platform for drug screening and development.

Science, this issue p. 920